Mediated Electrochemistry of Horseradish Peroxidase. Catalysis and Inhibition

ARTICLE *in* JOURNAL OF THE AMERICAN CHEMICAL SOCIETY · FEBRUARY 2002

Impact Factor: 12.11 · DOI: 10.1021/ja0170706 · Source: PubMed

J|A|C|S
ARTICLES
Published on Web 12/14/2001

Mediated Electrochemistry of Horseradish Peroxidase. Catalysis and Inhibition

Murielle Dequaire,[1] Benoît Limoges,* Jacques Moiroux,* and Jean-Michel Savéant*

Contribution from the Laboratoire d'Electrochimie Moléculaire de l'Université Denis Diderot (Paris 7), UMR CNRS 7591, 2 place Jussieu, 75251 Paris Cedex 05, France

Received September 13, 2001

Abstract: A precise determination of the complex mechanism of catalysis and inhibition involved in the reaction of HRP with H_2O_2 as substrate and an outersphere single electron donor ($[Os(bpy)_2pyCl]^+$) as cosubstrate is made possible by a systematic analysis of the cyclic voltammetric responses as a function of the scan rate and of the substrate and cosubstrate concentrations, complemented by spectrophotometric steady-state and stopped-flow experiments. The bell-shaped calibration curve relating the electrochemical response to the concentration of H_2O_2 is qualitatively and quantitatively explained by taking into account the conversion of the catalytically active forms of the enzyme into the inactive oxyperoxidase in addition to the primary catalytic cycle. These characteristics should be kept in mind in biosensor applications of HRP. The ensuing analysis and data allow one to predict biosensor amperometric responses in all practical cases. From a mechanistic standpoint, conditions may, however, be defined which render inhibition insignificant, thus allowing an electrochemical characterization of the primary catalytic cycle. At very low concentrations of H_2O_2, its diffusion tends to control the electrochemical response, resulting in proportionality with H_2O_2 concentration instead of the square root dependence characteristic of the classical catalytic currents. Intriguing hysteresis and trace crossings behaviors are also quantitatively explained in the framework of the same mechanism. As a consequence of the precise dissection of the rather complex reaction mechanism into its various elementary steps, a strategy may be devised for gaining a better understanding of the mechanism and reactivity patterns of each elementary step.

Heme peroxidases are ubiquitous enzymes that catalyze the oxidation of a broad range of substrates by hydrogen peroxide or by organic peroxides. Horseradish peroxidase (HRP) is an extracellular plant enzyme that partakes in regulation of cell growth and differentiation, polymerization of cell wall components, and the oxidation of secondary metabolites essential for important pathogenic defense reactions. Because of these essential functions, and also because of its stability and ready availability, HRP, particularly isoenzyme C, has been and continues to be one of the most studied enzymes.[2,3] HRP has been involved in a number of applications such as diagnostic assays,[4] biosensors,[5] bioremediation,[6] polymer synthesis,[7] and other biotechnological processes.[8] More applications are likely to be developed soon. Especially important will be those in which HRP catalysis can be translated into an electrochemical signal.

The normal catalytic cycle for HRP is shown in Scheme 1.[2] E_1 and E_2 are the oxidized states of the native ferriperoxidase (E), often referred as compounds I and II, respectively. Q is the reducing substrate and P its oxidized counterpart. The first step is a rapid oxygen atom transfer from hydrogen peroxide to the ferric porphyrin (Fe^{III}) of HRP (formally a $2e^-$ oxidation) to form the oxyferryl π-cation radical heme ($[Fe^{IV}{=}O]^{\bullet+}$) intermediate E_1 (iron formal oxidation state: +V) and water. In the second step, the porphyrin radical cation of compound I is reduced by the one-electron donor Q to yield the oxyferryl intermediate E_2 (iron formal oxidation state: +IV) and the product P. In the last step, the enzyme is converted back to its native resting state, E, by a subsequent one-electron/two-proton reduction of E_2 from a second molecule of Q to give a second equivalent of P and water.

(1) Present address: Laboratoire de Microbiologie Médicale et Moléculaire, Faculté de Médecine et de Pharmacie, 7 Boulevard Jeanne d'Arc, 21033 Dijon, France.

(2) (a) The recent book by Dunford[2b] provides an excellent account of the physical chemistry of heme peroxidases, including HRP, up to 1998. More recent publications[2c−i] attest of the continuously developing interest in the field. (b) Dunford, H. B. *Heme Peroxidases*; Wiley: New York, 1999. (c) Henriksen, A.; Smith, A. T.; Gajhede, M. *J. Biol. Chem.* **1999**, *274*, 35005. (d) Wang, W.; Noël, S.; Desmadril, M.; Guéguen, J.; Michon, T. *Biochem. J.* **1999**, *340*, 329. (e) Chen, S.-X.; Schopfer, P. *Eur. J. Biochem.* **1999**, *260*, 726. (f) Rodriguez-Lopez, J. N.; Gilabert, M. A.; Tudela, J.; Thorneley, R. N. F.; Garcia-Canovas, F. *Biochemistry* **2000**, *39*, 13201. (g) Filizola, M.; Loew, G. H. *J. Am. Chem. Soc.* **2000**, *122*, 18. (h) Hernandez-Ruiz, J.; Arnao, M. B.; Garcia-Canovas, F.; Acosta, M. *Biochem. J.* **2001**, *354*, 107. (i) Asokan, A.; de Ropp, J. S.; Newmyer, S. L.; Ortiz de Montellano, P. R.; La Mar, G. N. *J. Am. Chem. Soc.* **2001**, *123*, 4243.

(3) (a) Another area of active interest concerns oscillating systems involving HRP. For a recent review, see ref 3b. (b) Scheeline, A.; Olson, D. L.; Williksen, E. P.; Horras, G. A. *Chem. Rev.* **1997**, *97*, 739.

(4) Gosling, J. P. *Clin. Chem.* **1990**, *36*, 1408.

(5) Ruzgas, T.; Csöregi, E.; Emnéus, J.; Gorton, L.; Marko-Varga G. *Anal. Chim. Acta* **1996**, *330*, 123.

(6) (a) Klibanov, A. M.; Morris, E. D. *Enzyme Microb. Technol.* **1981**, *3*, 119. (b) Cooper, V. A.; Nicell, J. A. *Water Res.* **1996**, *30*, 954. (c) Wu, Y.; Taylor, K. E.; Biswas, N.; Bewtra, J. K. *Enzyme Microb. Technol.* **1998**, 22, 315.

(7) (a) Fukuoka, T.; Tonami, H.; Maruichi, N.; Uyama, H.; Kobayas, S.; Hideyuki, H. *Macromolecules* **2000**, *33*, 9152. (b) Durand, A.; Lalot, T.; Brigodiot, M.; Maréchal, E. *Polymer* **2000**, *41*, 8183.

(8) Colonna, S.; Gaggero, N.; Richelmi, C.; Pasta P. *Trends Biotechnol.* **1999**, *17*, 163.

10.1021/ja0170706 CCC: $22.00

Scheme 1

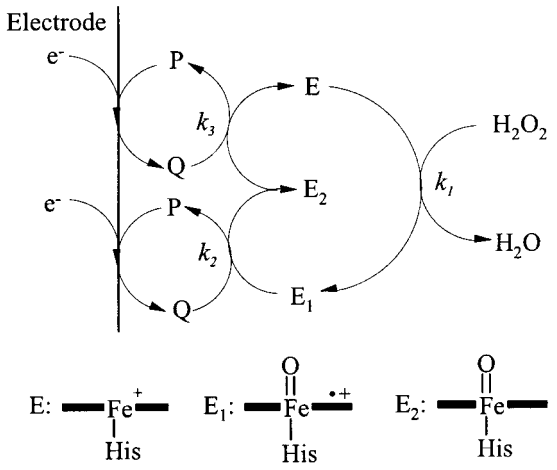

Scheme 1 also shows a possible connection of the enzymatic system with an electrode by means of a reversible one-electron mediator couple, P/Q, the reduced form of which, Q, serves as the cosubstrate to the enzyme. The electrochemical response may thus sense the amount of H_2O_2 present in the solution. A good sensitivity is thus expected at potentials where the direct reduction of H_2O_2 is negligible, since the electrochemical response should be enhanced by the catalytic properties of the enzyme. Alternatively, one may use the electrochemical response as a measure of the presence of the enzyme, again taking advantage of the good sensitivity offered by the catalytic properties of the enzyme. Several promising applications based on these principles have indeed been described, and more are likely to appear in the next future. For example, a variety of oxidases (e.g., glucose oxidase, choline oxidase, xanthine oxidase, catechol oxidase, pyruvate oxidase, cholesterol oxidase, etc.), which are able to produce hydrogen peroxide from molecular oxygen during the catalyzed oxidation of their substrates, have been coupled to horseradish peroxidase in several multienzyme amperometric biosensors.[9] HRP-based microelectrodes[10] were also developed for local monitoring of H_2O_2 generated photoelectrochemically,[10b] electrochemically, or enzymatically[10c] at surfaces. The main advantages were the excellent selectivity and sensitivity for H_2O_2 and, once adapted to a scanning electrochemical microscope, the possibility of imaging distributions of catalytic activity on the surface.[10c]

Most applications that exploit the catalytic current response to reveal the presence of HRP concern amperometric immunosensors in which HRP is used as an enzymatic label.[11] In these systems, the specific molecular recognition between an antigen and an antibody assembled on the electrode surface is translated into an electrochemical signal by means of the electrocatalytic activity of the HRP label attached to the immuno-complex. Based on a similar principle, an example of detection of specific DNA hybridization using an oligonucleotide probe labeled with HRP has recently been described.[12] It is also important to note that promising approaches based on scanning electrochemical microscopy have recently been developed for imaging localized HRP on surfaces,[13] thereby offering new opportunities in the field of multianalyte immunoassays.[13b]

Transduction of HRP catalysis into an electrochemical signal[5] may involve direct electron transfer from the electrode to the oxidized forms of HRP.[14,15] It may also make use of a mediator that shuttles electrons from the electrode (Scheme 1) to the enzyme, which is either present in the solution[15,16] or immobilized onto the electrode surface.[15,17] In other systems, the enzyme is "wired" to the electrode by means of an electron-hopping redox polymer or hydrogel or by other conducting systems.[18,19]

The cyclic voltammetric behavior depicted in Figure 1 is anticipated for a simple catalytic mechanism, involving a reversible mediator couple, P/Q, in which the rate-determining

(9) (a) For an introductory text on biosensors, see ref 9b. (b) Turner, A. P. F.; Karube, I.; Wilson, G. S. *Biosensors. Fundamentals and Applications*; Oxford University Press: New York, 1987. (c) Garguilo, M. G.; Huynh, N.; Michael, A. C. *Anal. Chem.* **1993**, *65*, 523. (d) Kulys, J. J.; Schmid, R. D. *Bioelectrochem. Bioenerg.* **1990**, *24*, 305. (e) Tatsuma, T.; Watanabe, T.; Watanabe, T. *J. Electroanal. Chem.* **1993**, *356*, 245. (f) Buttler, T. A.; Johansson, K.; Gorton, L.; Marko-Varga, G. A. *Anal. Chem.* **1993**, *65*, 2628. (g) Kacaniklick, V.; Johanson, K.; Marko-Varga, G.; Gorton, L.; Jönsson-Pettersson, G.; Czöregi, E. *Electroanalysis* **1994**, 6, 381.

(10) (a) Pantano, P.; Morton, T. H.; Kuhr, W. G. *J. Am. Chem. Soc.* **1991**, *113*, 1832. (b) Sakai, H.; Baba, R.; Hashimoto, K.; Fujishima, A.; Heller, A. *J. Phys. Chem.* **1995**, *99*, 11896. (c) Horrocks, B. J.; Schmidtke, D.; Heller, A.; Bard, A. J. *Anal. Chem.* **1993**, *65*, 3605.

(11) (a) Deasy, B.; Dempsey, E.; Smyth, M. R.; Egan, D.; Bogan, D.; O'Kennedy, R. *Anal. Chim. Acta* **1994**, *294*, 291. (b) Pritchard, D. J.; Morgan, H.; Cooper, J. M. *Anal. Chim. Acta* **1995**, *310*, 251. (c) McNeil, C. J.; Athey, D.; Ho, W. O. *Biosens. Bioelectron.* **1995**, *10*, 75. (d) Del Carlo, M.; Mascini, *Anal. Chim. Acta* **1996**, *336*, 167. (e) Rishpon, J.; Ivnitski, D. *Biosens. Bioelectron.* **1997**, *12*, 195. (f) Campbell, C. N.; Lumley-Woodyear, T.; Heller, A. *Fresenius J. Anal. Chem.* **1999**, *364*, 165. (g) Chetcuti, A. F.; Wong, D. K. Y.; Stuart, M. C. *Anal. Chem.* **1999**, *71*, 4088.

(12) (a) Caruana, D. J.; Heller, A. *J. Am. Chem. Soc.* **1999**, *121*, 769. (b) Lumley-Woodyear, T.; Caruana, D. J.; Campbell, C. N.; Heller, A. *Anal. Chem.* **1999**, *71*, 394.

(13) (a) Kasai, S.; Yokota, A.; Zhou, H.; Nishizawa, M.; Niwa, K.; Onouchi, T.; Matsue, T. *Anal. Chem.* **2000**, *72*, 5761. (b) Shiku, H.; Hara, Y.; Matsue, T.; Uchida, I.; Yamauchi, T. *J. Electroanal. Chem.* **1997**, *438*, 187. (c) Zhou, H.; Kasai, S.; Matsue, T. *Anal. Biochem.* **2001**, *290*, 83.

(14) (a) Paddock, R. M.; Bowden, E. F. *J. Electroanal. Chem.* **1989**, *260*, 487. (b) Wollenberger, U.; Wang, J.; Ozsoz, M.; Gonzales-Romero, E. *Bioelectrochem. Bioenerg.* **1991**, *26*, 287. (c) Tatsuma, T.; Watanabe, T. *Anal. Chem.* **1991**, *63*, 1580. (d) Ho, W. O.; Athey, D.; McNeil, C. J.; Hager, H. J.; Evans, G. P.; Mullen, W. H. *J. Electroanal. Chem.* **1993**, *351*, 185. (e) Csöregi, E.; Emnéus, J.; Gorton, L.; Marko-Varga, G.; Tüdös, A. J.; Kok, W. T. *Anal. Chem.* **1994**, *66*, 3604. (f) Scott, D. L.; Bowden, E. F. *Anal. Chem.* **1994**, *66*, 1217. (g) Ruzgas, T.; Emnéus, J.; Gorton, L.; Marko-Varga G. *J. Electroanal. Chem.* **1995**, *391*, 41. (h) Wang, J.; Freiha, B.; Naser, N.; Gonzales-Romero, E.; Wollenberger, U.; Ozsoz, M.; Evans, O. *Anal. Chim. Acta* **1996**, *330*, 123. (i) Mondal, M. S.; Goodin, D. B.; Armstrong, F. A. *J. Am. Chem. Soc.* **1998**, *120*, 6270. (j) Heering, H. A.; Hiirst, J.; Armstrong, F. A. *J. Phys. Chem. B* **1998**, *102*, 6889. (k) Tatsuma, T.; Ariyama, K.; Oyama, N. *J. Electroanal. Chem.* **1998**, *446*, 205. (l) Xiao, Y.; Ju, H.-X.; Chen, H.-Y. *Anal. Chim. Acta* **1999**, *391*, 73. (m) Lingren, A.; Ruzgas, T.; Gorton, L.; Csöregi, E.; Ardila, G. B.; Sakharov, I. Y.; Gazaryan, I. G. *Biosens. Bioelectron.* **2000**, *15*, 491. (n) Chen, X.; Ruan, C.; Kong. J.; Deng, J. *Anal. Chim. Acta* **2000**, *412*, 89.

(15) In several instances, cytochrome *c* peroxidase is used in place of HRP, both enzymes exhibiting similar behaviors.

(16) (a) Frew, J. E.; Harmer, M. A.; Hill, H. A. O.; Libor, S. I. *J. Electroanal. Chem.* **1986**, *201*, 1. (b) Smit, M. H.; Cass, A. E. G. *Anal. Chem.* **1990**, *62*, 2429. (c) Cooper, J. M.; Bannister, J. V.; McNeil, C. J. *J. Electroanal. Chem.* **1991**, *312*, 155. (d) Nakabayashi, Y.; Omayu, A.; Morii, S.; Yagi, S. *Sens. Actuators B* **2000**, *66*, 128.

(17) (a) Sànchez, P. D.; Ordierez, A. J. M.; Garcia, A. C.; Blanco, P. T. *Electroanalysis* **1991**, *3*, 281. (b) Wollenberger, U.; Drungiliene, A.; Stöcklein, W.; Kulys, J. J.; Scheller, F. W. *Anal. Chim. Acta* **1996**, *329*, 231. (c) Tatsuma, T.; Okawa, Y.; Watanabe, T. *Anal. Chem.* **1989**, *61*, 2352. (d) Tsai, W.-C.; Cass, A. E. G. *Analyst* **1995**, *120*, 2249. (e) Sun, C.; Li, W.; Sun, Y.; Zhang, X.; Shen, J. *Electrochim. Acta* **1999**, *44*, 3401. (f) Okawa, Y.; Nagano, M.; Hirota, S.; Kobayashi, H.; Ohno, T.; Watanabe, T. *Biosens. Bioelectron.* **1999**, *14*, 229. (g) Razola, S. R.; Aktas, E.; Viré, J.-C.; Kauffmann, J.-M. *Analyst* **2000**, 125, 79.

(18) (a) Vreeke, M.; Maidan, R.; Heller, A. *Anal. Chem.* **1995**, *67*, 303. (b) Vreeke, M.; Rocca, P.; Heller, A. *Anal. Chem.* **1995**, *67*, 303. (c) Lumley-Goodyear, T.; Rocca, P.; Lindsay, J.; Dror, Y.; Freeman, A.; Heller, A. *Anal. Chem.* **1995**, *67*, 1332. (d) Vreeke, M.; Yong, K. T.; Heller, A. *Anal. Chem.* **1995**, *67*, 4247.

(19) (a) Kulys, J.; Bilitewski, U.; Schmid, R. D. *Bioelectrochem. Bioenerg.* **1991**, *26*, 277. (b) Tatsuma, T.; Gondaira, M.; Watanabe, T. *Anal. Chem.* **1992**, *64*, 1183. (c) Mulchandani, A.; Wang, C.-L.; Weetall, H. H. *Anal. Chem.* **1995**, *67*, 94. (d) Wendzinski, F.; Gründig, Renneberg, R.; Spener, F. (e) Ruan, C.; Yang, F.; Lei, C.; Deng, J. *Anal. Chem.* **1998**, *70*, 1721. (f) Bartlett, P. N.; Birkin, P. R.; Wang, J. H. *Anal. Chem.* **1998**, *70*, 3685. (g) Gaspar, S.; Habermüller, K.; Csöregi, E.; Schuhmann, W. *Sens. Actuators B* **2001**, *72*, 63.

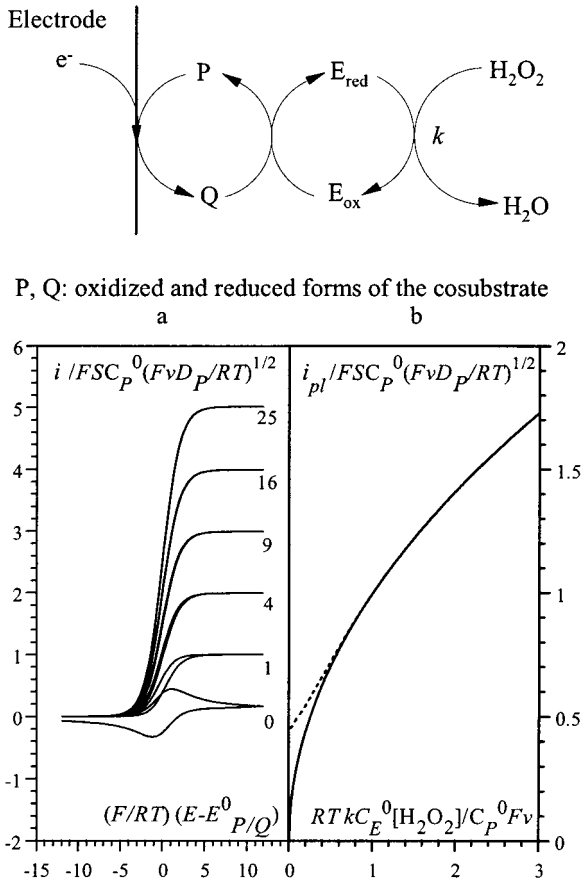

Figure 1. Cyclic voltammetry of a standard catalytic mechanism where the rate-determining step (rate constant: k) is first order in H_2O_2 (top scheme). (a) Cyclic voltammogram obtained upon increasing the parameter $RTkC_E^0C_S^0/F\nu C_P^0$. (b) variation of the peak (dotted line) or the plateau current (full line) with the same parameter.

step is first order in H_2O_2. Upon increasing the parameter $\lambda = RTkC_E^0C_S^0/F\nu C_P^0$ (C_E^0, enzyme concentration in moles per liter; C_S^0, C_P^0, bulk concentrations of the substrate S (i.e., H_2O_2) and cosubstrate in moles per cubic centimeter; k, overall rate constant in moles per liter per second; ν, scan rate in volts per second), the reversible wave of the cosubstrate becomes irreversible and plateau-shaped and increases in height as represented in Figure 1.[20] The parameter λ measures the competition between the rate of the catalytic reaction numerator and the rate of diffusion (itself governed by the scan rate). Thus, at low H_2O_2 concentrations, low values of the controlling rate constant, and/or high scan rates, the electrochemical response is simply the diffusion-controlled reversible voltammogram of the cosubstrate, containing no information on the catalytic process and no dependence on the H_2O_2 concentration. Conversely, at high substrate concentrations, high values of the controlling rate constant, and/or low scan rates, the voltammogram becomes S-shaped and independent of scan rate. Under these conditions, the calibration curve (Figure 1b) relating the peak or plateau current to the concentration of H_2O_2 has no reason to be a straight line. The plateau current rather varies with the square root of H_2O_2 concentration. Once these criteria are met, the rate constant k may be derived straightforwardly from the plateau current, i_{pl}, according to eq 1. (F, Faraday constant; S, electrode surface

$$i_{pl} = FS\sqrt{D_P}\sqrt{kC_E^0C_P^0C_S^0} \qquad (1)$$

area in square centimeters; D_P, diffusion coefficient of the cosubstrate in square centimeters per second). If these criteria are not fulfilled, rate constants derived from brute force application of eq 1 have no definite meaning.

In the case of an immobilized enzyme, the voltammograms are expected to be similar to what is shown in Figure 1 for a monolayer or for a multilayer system under conditions where charge propagation through the film is fast, letting the catalytic reaction be the sole rate-determining step within the film.[21,22] Although the expression of the plateau current is a little different from the solution case, its expected variation with H_2O_2 concentration is likewise nonlinear.

It should be noted that the plateau current (independent of the scan rate) in cyclic voltammetry that we just analyzed is the same as the current (independent of time) obtained upon stepping the electrode potential on the plateau. If a rotating disk technique is used, the catalytic plateau current is expected to be independent of the rotation rate and exactly equal to the cyclic voltammetric current or the potential-step current. In the competition with diffusion of the cosubsrate depicted by the parameter λ, $RT/F\nu$ is replaced by the time, t, in potential-step experiments and by δ^2/D_P in rotating disk experiments (δ is the thickness of the diffusion layer in centimeters).

We may now examine the rare attempts at quantitative analyses available in the literature with reference to the expected behavior just described. Generally speaking, the expected variations of the measured current with H_2O_2 concentration are practically never found. Scan-rate-independent plateau-shaped curves are found with solutions of cytochrome *c* peroxidase and 2-aminoethylferrocene containing 0.2 mM H_2O_2.[16a] However, for lower H_2O_2 concentrations, stepping the potential at the plateau level does not result in a steady-state current but rather a current decaying with time, the maximum current being proportional to H_2O_2 concentration.[16a] Unexplained linear variations of the current with H_2O_2 concentration, at low values, have been observed in several cases under various mass transport conditions.[17g,18a,19d] That complex mechanisms are operating is attested by the trace-crossing curves observed, for example, with HRP in the presence of a mediator in solution upon addition of 5 mM H_2O_2.[9c] Apparent Michaelis−Menten kinetics has been invoked to rationalize saturation behavior appearing upon increasing H_2O_2 concentration.[11a,17c,h] Inhibition has been likewise broadly invoked, with no further precision, as an explanation for the few reported cases where a decrease of the electrochemical response upon raising the H_2O_2 concentration was observed.[9c,19f]

(20) (a) Savéant, J.-M.; Vianello, E. In *Advances in Polarography*; Longmuir, I. S., Ed.; Pergamon Press: London, 1960; Vol. 1, pp 367−374. (b) Andrieux, C. P.; Savéant, J.-M. In *Electrochemical Reactions in Investigation of Rates and Mechanisms of Reactions; Techniques of Chemistry*; Bernasconi, C. F., Ed.; Wiley: New York, 1986; Vol. VI/4E, Part 2, pp 305−390. (c) Savéant, J.-M.; Su, K. B. *J. Electroanal. Chem.* **1984**, *171*, 341. (d) Bourdillon, C.; Demaille. C.; Moiroux, J.; Savéant, J.-M. *J. Am. Chem. Soc.* **1993**, *115*, 2.

(21) (a) Andrieux, C. P.; Savéant, J.-M. *Catalysis at redox polymer coated electrodes* in *Molecular Design of Electrode Surfaces*; Murray, R. W., Ed.; Techniques in Chemistry 22; Wiley: New York, 1992; pp 207−270. (b) Bourdillon, C.; Demaille. C.; Gueris, J.; Moiroux, J.; Savéant, J.-M. *J. Am. Chem. Soc.* **1993**, *115*, 11264.

(22) The combination of the cosubstrate diffusion and catalytic reaction is somewhat different since they now take place within two separate portions of space. The resulting expression of the current is in fact simpler since it is given by a simple addition of the two phenomena.

To be put on sound quantitative bases, most of the applications of HRP-mediated electrochemistry that we have evoked earlier, as well as likely developments in the field, require a precise knowledge of the relationship between the amount of substrate, cosubstrate, and enzyme present in the solution and of the underlying mechanisms. The various unexplained odd behaviors that we have listed above illustrate the lack of such knowledge at present. Deciphering and quantitatively characterizing the complex mechanism that governs the electrochemical responses of HRP in the presence of H_2O_2 and of a reversible cosubstrate couple was the main task of the work described below. To avoid further complication, we selected a reversible fast one-electron couple, $[Os(bpy)_2pyCl]^{2+}/[Os(bpy)_2pyCl]^{+}$, involving no proton transfer. We also decided to start our study with the case where the enzyme is present in the solution, rather than immobilized on the electrode surface, in the aim of disposing of a quantitatively analyzed mechanism, deprived of any of the ambiguities that may arise from the immobilization procedure, to serve as reference for future studies.

This description of the mediated electrochemistry of HRP in the presence of its substrate was also the occasion of a journey through almost all facets of catalysis and inhibition exhibited by this enzyme. They indeed jointly act to determine the electrochemical response, making electrochemistry a particularly valuable mode of activating these types of systems. Another outcome of the work is the definition of the conditions under which mediated electrochemistry may serve to determine some of the key rate constants and thus contribute to a better understanding of HRP reactivity.

Results and Discussion

Broad Features of the Cyclic Voltammetry of HRP in the Presence of H_2O_2 (Substrate) and $[Os(bpy)_2pyCl]^{2+}$ (Cosubstrate). Figure 2a shows a typical set of voltammograms obtained at 0.05 V s^{-1} with increasing concentrations of H_2O_2 (Figure 2b shows the corresponding simulated curves as discussed later on).[23] These curves were recorded 20 min after the mixing of the reactants so as to ensure that a steady state between the various forms of the enzyme is established before starting the potential scan. We start from the reversible voltammogram of the osmium(III) complex in the absence of hydrogen peroxide. Upon addition of H_2O_2, the peak current increases while the wave becomes irreversible. At higher values of H_2O_2 concentration, the peak tends to disappear, the wave becoming S-shaped with the forward and reverse traces almost superimposed. Upon increasing further the H_2O_2 concentration, the plateau current decreases and a peak finally reappears. It is striking that, at the upper end of the range of H_2O_2 concentrations, the wave has become almost completely reversible, practically the same as when there was no H_2O_2 in the solution. The upward and then downward variations of the peak or plateau current with the concentration of H_2O_2 are summarized in Figure 2c, for this value of the scan rate. One of our first tasks is to disclose the reasons for this unusual behavior. The effect of the scan rate is also intriguing, as can be seen in the examples given in Figure 3.

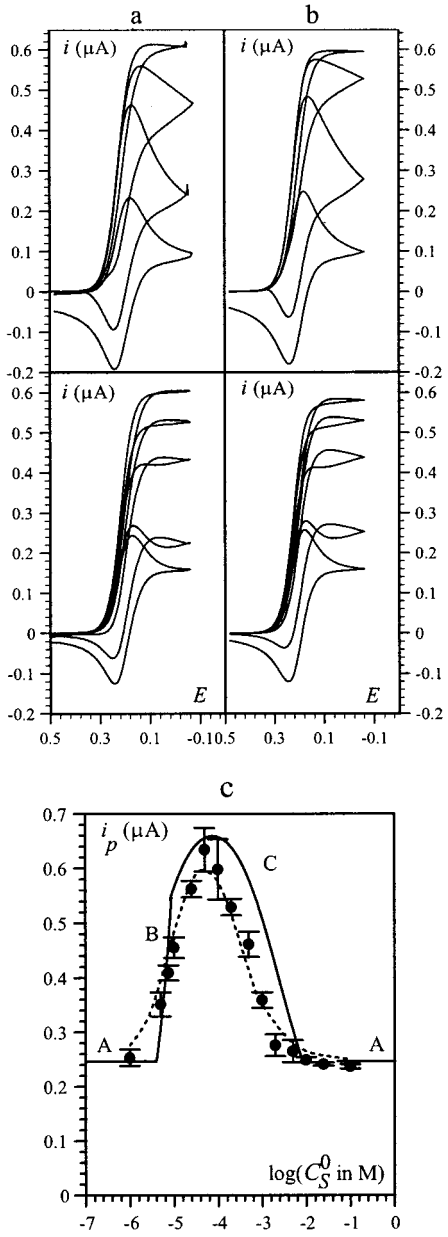

Figure 2. (a) Cyclic voltammograms (scan rate: 50 mV s^{-1}) recorded in a phosphate buffer solution (pH 7.4) containing 20 μM $[Os(bpy)_2pyCl]^{2+}$, 0.2 μM HRP, and increasing concentrations of H_2O_2 (upper curves, from bottom to top, 0, 0.01, 0.025, 0.05 mM; lower curves, from top to bottom, 0.1, 0.2, 0.5, 5, 25 mM). The scan is started ca. 20 min after mixing the reactants (see text). (b) Corresponding simulated curves (for details, see text). *E* in volts vs SCE. (c) Variation of the peak or plateau (when there is no peak) current with the concentration of H_2O_2. Filled circle symbol: experimental average value of 3−10 measurements per data. The vertical bars are the standard deviations. Full lines: theoretical curves in the case of (A) absence of catalysis; (B) control by H_2O_2 diffusion (total catalysis); (C) plateau current according to eq 6. Dotted line: finite difference simulation.

At a given concentration of H_2O_2, decreasing the scan rate tends to convert peaks into plateaus. Also, at low scan rates, hysteresis appears: on the forward scan there seems to be delay time for reaching the plateau. In the region of the plateau, the current on the reverse scan is then higher than that on the forward scan, before decreasing upon approaching the standard potential of the mediator and going further beyond. This hysteresis behavior is coupled with crossing of the cathodic and anodic traces, the crossing phenomenon becoming more and

(23) The voltammetric curves and the peak currents were all corrected for the capacitive background current obtained in pure electrolyte. The reversible wave of the $[Os(bpy)_2pyCl]^{2+}$ compound indicates a standard potential of 0.210 V vs SCE.

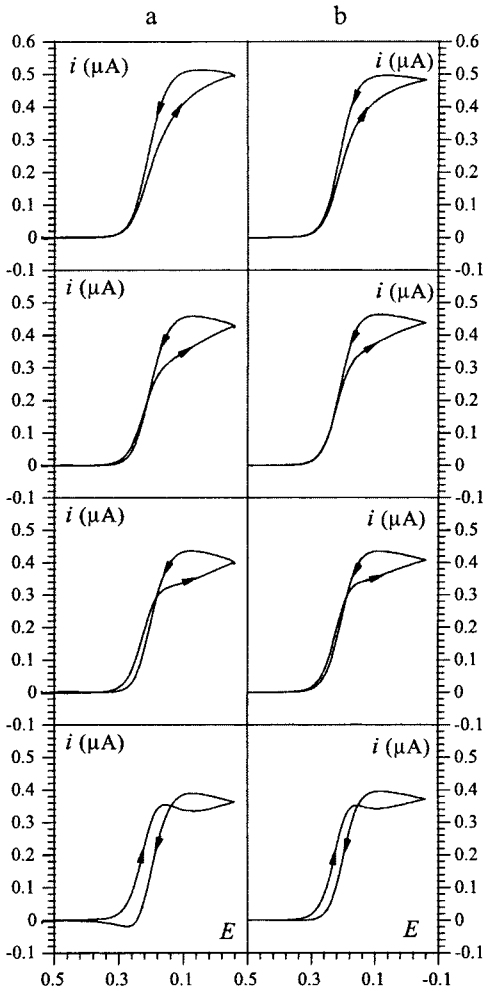

Figure 3. (a) Cyclic voltammograms recorded at different scan rates in a phosphate buffer solution (pH 7.4) containing 20 μM $[Os(bpy)_2pyCl]^{2+}$, 0.2 μM HRP, and 1 mM H_2O_2 after attainment of the steady state before starting the potential scan. Scan rates, from top to bottom: 10, 20, 30, 50 mV s^{-1}. (b) Corresponding simulated curves (for details see text). *E* in volts vs SCE.

more apparent as the scan rate is raised. Explaining hysteresis and trace crossing is another challenging task.

Outline of the Step-by-Step Mechanistic Analysis. Our attempt to unravel the mechanism of the catalytic reaction was based on the variations of the electrochemical response with the concentrations of substrate and cosubstrate and with the scan rate. There is little doubt that the decrease in the catalytic current observed upon raising the concentration of H_2O_2 is due to some form of inhibition of the enzyme. In view of its complexity, it seems necessary to proceed by a step-by-step analysis of the mechanism.

We will look first for conditions where inhibition may be neglected so as to establish the electrochemical response resulting solely from the three-cornered catalytic cycle depicted in Scheme 1. This preliminary analysis, complemented with a series of spectrophotometric steady-state and stopped-flow experiments, will lead to the determination of the kinetic characteristics of the reactions of the reduced form of the cosubstrate, $[Os(bpy)_2pyCl]^+$, with the E_1 and E_2 forms of the enzyme.

In a second stage, it will be shown that inhibition by formation of the oxyperoxidase form (E_3) of the enzyme explains the

Scheme 2

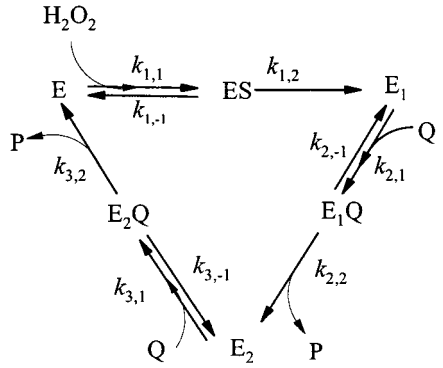

observations made at high H_2O_2 concentrations, taking into account that the cosubstrate may reduce E_3 back to the active form E_1, thus restarting the primary catalytic cycle.

In a third step, we will come back to the very low concentrations of H_2O_2 and explain why a peak rather than a plateau is then observed. The mechanistic and kinetic information obtained at this stage will then be used to explain the occurrence of hysteresis and trace crossings, as exemplified by the curves shown in Figure 3, emphasizing the delay required for the mutual transformation of the various enzyme forms to reach a steady state.

All pieces of knowledge successively obtained will finally be assembled to provide a comprehensive description of the reaction mechanism over the whole range of H_2O_2 concentrations.

Determination of the rate constants pertaining to inhibition and reactivation of the inhibited enzyme will necessitate an iterative treatment of the data depicted in the second and fourth parts of the above sections. The first step of the analysis required that conditions be defined under which inhibition may be neglected. For the sake of self-consistency, a last paragraph will therefore be devoted to testing that this is indeed the case for both steady-state spectrophotometric and cyclic voltammetric experiments.

Uninhibited Catalysis. Kinetic Characteristics of the Reaction of the Reduced Form of the Cosubstrate, $[Os(bpy)_2pyCl]^+$, with the E_1 and E_2 Forms of the Enzyme. In the primary catalytic cycle of HRP (Scheme 2), the kinetics of the reaction of E with H_2O_2 to yield E_1 has been investigated extensively.[2] Although evidence has been previously gathered that the kinetics follows a Michaelis−Menten behavior,[24] it is only recently that its characteristics have been unambiguously determined,[2f] leading to $K_{1,M} = (k_{1,-1} + k_{1,2})/k_{1,1} = 128$ μM and to a confirmation of the k_1 value, i.e., $k_1 = k_{1,1}k_{1,2}/(k_{1,-1} + k_{1,2}) = 1.7 \times 10^7$ M^{-1} s^{-1}. The reduction of E_1 and E_2 by several electron donors has been reported, although they are in most cases both electron and proton donors, unlike the osmium cosubstrate investigated in the present study. Recent work in this area[25] has shown that, with phenol derivatives as electron donors, the reduction of E_1 is much faster than the reduction of E_2, a result found with many other electron donors.[2c,26] We found

(24) (a) A Michaelis−Menten behavior was observed at low temperature by stopped-flow cryoenzymology.[24b] After extrapolation at 25 °C, a value of $K_{1,M} = 46$ μM has been proposed. (b) Baek, H. K.; Van Wart, H. E. *Biochemistry* **1989**, *28*, 5714.

(25) (a) Folkes, L. K.; Candeias, L. P. *FEBS Lett.* **1997**, *412*, 305. (b) Khopde, S. M.; Priyadarsini, K. I. *Biophys. Chem.* **2000**, *88*, 103.

the same with the $[Os(bpy)_2pyCl]^+$ cosubstrate in the stopped-flow experiments depicted below. Scheme 2 indicates the possibility of a Michaelis−Menten behavior also for the reduction of E_1 and E_2 in view of the fact that such behavior has been reported for several other cosubstrates.[2d,f]

(i) Stopped-Flow Spectrophotometric Experiments. Because of the intense adsorption of the osmium(II) complex in the Soret region and because of the rate limitations of the instrument (500 s^{-1}), the kinetics were monitored only under second-order conditions. Values of $k_2 = k_{2,1}k_{2,2}/(k_{2,-1} + k_{2,2}) = (2.0 \pm 0.5) \times 10^8$ M^{-1} s^{-1} and of $k_3 = k_{3,1}k_{3,2}/(k_{3,-1} + k_{3,2}) = (1.0 \pm 0.2) \times 10^7$ M^{-1} s^{-1} were found for reductions of E_1 and E_2, respectively, showing that the reduction of E_1 is ~20-fold faster than the reduction of E_2.

(ii) Steady-State Spectrophotometry. The decay of the concentration of $[Os(bpy)_2pyCl]^+$ was followed by the variation of the osmium(II) band at 500 nm. The recording started immediately after addition of 0.1 mM H_2O_2. Under these conditions, the slow (rate constant: 2.5×10^{-3} s^{-1} [2h]), irreversible deactivation of the enzyme to the verdohemoporphyrin (P670) may be neglected. As shown in detail in the last section of this paper, the conversion of the initial enzyme by H_2O_2 into inactive oxyperoxidase may likewise be neglected. The variation of the initial rate, v_0, with the initial concentration of $[Os(bpy)_2pyCl]^+$ was fitted as shown in Figure 4 with Michaelis−Menten-type kinetics. More precisely, the expression of the initial rate corresponding to the reaction scheme depicted in Scheme 2 is given by eq 2, assuming that Michaelis−Menten-

$$v_0 = -\left(\frac{d[Q]}{dt}\right)_{t=0} = (k_{2,1}[Q]_{t=0}[E_1] - k_{2,-1}[E_1Q]) + (k_{3,1}[Q]_{t=0}[E_2] - k_{3,-1}[E_2Q]) \quad (2)$$

type kinetics are followed for the reactions of the cosubstrate with E_1 and E_2. When the various forms of the enzyme have reached a steady-state distribution, the initial rate is given (see Supporting Information) by any of the three equivalent forms of eq 3. The K_M's are the Michaelis−Menten constants. Since,

$$\frac{2C_E^0}{v_0} = \frac{1}{k_{3,2}}\left(1 + \frac{k_{3,-1} + k_{3,2}}{k_{3,1}[Q]_{t=0}}\right) + \frac{1}{k_{2,2}}\left(1 + \frac{k_{2,-1} + k_{2,2}}{k_{2,1}[Q]_{t=0}}\right) + \frac{1}{k_{1,2}}\left(1 + \frac{k_{1,-1} + k_{1,2}}{k_{1,1}C_S^0}\right)$$

$$= \frac{1}{k_{3,2}}\left(1 + \frac{K_{3,M}}{[Q]_{t=0}}\right) + \frac{1}{k_{2,2}}\left(1 + \frac{K_{2,M}}{[Q]_{t=0}}\right) + \frac{1}{k_{1,2}}\left(1 + \frac{K_{1,M}}{C_S^0}\right)$$

$$= \frac{1}{k_{3,2}} + \frac{1}{k_3[Q]_{t=0}} + \frac{1}{k_{2,2}} + \frac{1}{k_2[Q]_{t=0}} + \frac{1}{k_{1,2}} + \frac{1}{k_1C_S^0} \quad (3)$$

as derived from the stopped-flow experiments, the E_1/E_2 reaction is much faster than the E_2/E reaction, the second group of terms in eq 3 may be neglected, leading to eq 4. Application of this

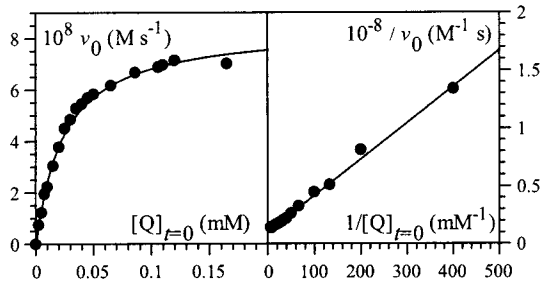

Figure 4. Reaction of HRP (0.2 nM) with $[Os(bpy)_2pyCl]^+$ in the presence of 0.1 mM H_2O_2 in a phosphate buffer solution (pH 7.4). Dependence of the initial rate, v_0 (from the decay of Q monitored at 500 nm), on the initial concentration $[Q]_{t=0}$. Left: direct plot. Right: reciprocal plot.

Table 1. Derivation of the Kinetic Characteristics of the E_2/E Reaction[a]

$k_3 \times 10^{-7}$ (M^{-1} s^{-1})	$k_{3,2}$ (s^{-1})	$K_{3,M}$ (μM)
From the reciprocal plot of the spectrophotometric data in Figure 4		
0.8	300 (230)	37 (28)
From the cyclic voltammetric data in Figure 6		
1.4	280 (230)	20 (17)

[a] Values in parentheses were obtained under the assumption that reaction E/E_1 is much faster than reaction E_2/E.

$$\frac{2C_E^0}{v_0} = \frac{1}{k_{3,2}}\left(1 + \frac{k_{3,-1} + k_{3,2}}{k_{3,1}[Q]_{t=0}}\right) + \frac{1}{k_{1,2}}\left(1 + \frac{k_{1,-1} + k_{1,2}}{k_{1,1}C_S^0}\right)$$

$$= \frac{1}{k_{3,2}}\left(1 + \frac{K_{3,M}}{[Q]_{t=0}}\right) + \frac{1}{k_{1,2}}\left(1 + \frac{K_{1,M}}{C_S^0}\right)$$

$$= \frac{1}{k_{3,2}} + \frac{1}{k_3[Q]_{t=0}} + \frac{1}{k_{1,2}} + \frac{1}{k_1C_S^0} \quad (4)$$

equation to the experimental data through the construction of a reciprocal plot (Figure 4), using the literature values, $k_1 = 1.7 \times 10^7$ M^{-1} s^{-1} and $k_{1,2} = 2170$ s^{-1},[2f] leads to the results summarized in Table 1, showing that the value of k_3 is in good agreement with the result of the stopped-flow experiments. It is also seen in Table 1 that the assumption that the reaction E/E_1 is much faster than the reaction E_2/E does not change the results dramatically. It follows that uncertainties in the determination of the kinetic parameters of reaction E/E_1, like the value of its Michaelis constant, will not have much effect on the values characterizing the reaction E_2/E.

Concerning the Michaelis−Menten behavior observed for the E_2/E reaction, it should be emphasized that the reduction of E_2 is not a mere outersphere electron-transfer reaction but rather involves the exchange of one electron and two protons and the cleavage of the iron−oxygen bond (Scheme 3). These reactions, or maybe other mechanistic peculiarities to be uncovered, might be the cause of the observed kinetics showing saturation behavior upon increasing the reactant concentration, which therefore does not necessarily reflect a true Michaelis−Menten mechanism such as the one depicted in Scheme 2

(iii) Cyclic Voltammetry. How does the reaction E_2/E manifest itself through the cyclic voltammetric catalytic currents? That is the question we address now. Inhibition by conversion of the initial enzyme by H_2O_2 into inactive oxyperoxidase, E_3, may occur even in the presence of the oxidized form of the cosubstrate. H_2O_2 may indeed reduce E_1 into E_2,

(26) (a) Goral, V. N.; Ryabov, A. D. *Biochem. Mol. Biol. Int.* **1998**, *45*, 61. (b) Cormier, M.; Prihard, P. *J. Biol. Chem.* **1968**, *243*, 4706. (c) Hasinoff, F.; Dunford, H. B. *Biochemistry* **1970**, *9*, 4930. (d) Dunford, H. B.; Cotton, M. L. *J. Biol. Chem.* **1975**, *250*, 2920. (e) Dunford, H. B.; Job, D. *Eur. J. Biochem.* **1976**, *66*, 607.

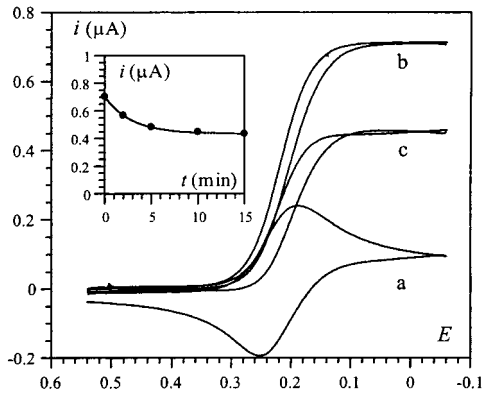

Figure 5. Cyclic voltammograms obtained at 50 mV s^{-1} in a phosphate buffer (pH 7.4) containing (a) 20 μM $[Os(bpy)_2pyCl]^+$ alone; (b,c) 20 μM $[Os(bpy)_2pyCl]^+$, 0.2 μM HRP, and 0.2 mM H_2O_2. The curve was recorded (b) immediately after the addition of the three components and (c) after an incubation time of 15 min. Inset: dependence of the plateau current on the incubation time.

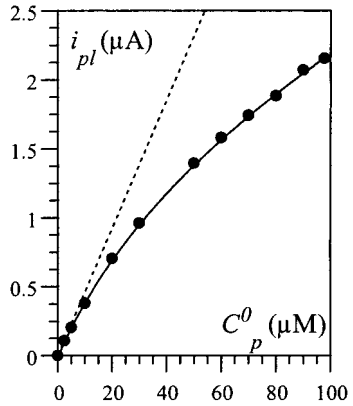

Figure 6. Catalytic plateau current as a function of the cosubstrate concentration recorded at 50 mV s^{-1} just after mixing in a phosphate buffer (pH 7.4) containing 0.2 μM HRP and 0.2 mM H_2O_2. Full line: fitting with a Michaelis−Menten kinetics according to eq 6. Dotted line: low concentration linear variation (eq 7).

Scheme 3

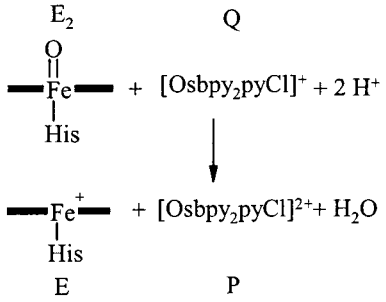

albeit slowly,[2h] thus opening a route to the conversion of E_2 into E_3. This is the reason for the slow decay of the catalytic current observed in Figure 5, which can therefore be avoided by running the cyclic voltammogram immediately after addition of H_2O_2 to the mixture of HRP and osmium(III). Conversion of E_2 into E_3 by reaction with H_2O_2 can nevertheless occur during the recording of the voltammogram. We will come back to this point at the end of the paper and show that the conversion is negligible under the conditions depicted below that were used to investigate the kinetics of the E_2/E reaction.

The rate law governing the catalytic system is the same as in eq 4, replacing $[Q]_{t=0}$ by [Q]. It follows that the diffusion reaction equation governing the variations of [Q] with space (x) and time (t) is given by eq 5 in the framework of linear

$$\frac{\partial[Q]}{\partial t} = D_P\frac{\partial^2[Q]}{\partial x^2} - \frac{2C_E^0k_3[Q]}{1 + k_3[Q]\left(\frac{1}{k_{3,2}} + \frac{1}{k_{1,2}} + \frac{1}{k_1C_S^0}\right)} \quad (5)$$

diffusion (other equivalent forms may be derived from eq 4), with as initial and boundary conditions $x \geq 0$, $t = 0$, and $x = \infty$, $t \geq 0$, $[Q] = 0$; $x = 0$, $t \geq 0$, $[Q] = C_P^0$, on the plateau of the cyclic voltammetric wave. The plateau current, $i_{pl} = FSD_P(\partial[Q]/\partial x)_{x=0}$, is thus given by eq 6 (see Supporting Information).

$$i_{pl} = FS\sqrt{\frac{4C_E^0C_P^0D_P}{\frac{1}{k_{3,2}} + \frac{1}{k_{1,2}} + \frac{1}{k_1C_S^0}}\left\{1 - \frac{\ln\left[1 + k_3C_P^0\left(\frac{1}{k_{3,2}} + \frac{1}{k_{1,2}} + \frac{1}{k_1C_S^0}\right)\right]}{k_3C_P^0\left(\frac{1}{k_{3,2}} + \frac{1}{k_{1,2}} + \frac{1}{k_1C_S^0}\right)}\right\}} \quad (6)$$

At low concentrations of cosubstrate, the plateau current varies in proportion to C_P^0 according to eq 7, whereas a saturation

$$i_{pl} = FS\sqrt{D_P}C_P^0\sqrt{2k_3C_E^0} \quad (7)$$

value is reached (eq 8) at high C_P^0.

$$i_{pl} = FS\sqrt{\frac{4C_E^0C_P^0D_P}{\frac{1}{k_{3,2}} + \frac{1}{k_{1,2}} + \frac{1}{k_1C_S^0}}} \quad (8)$$

These equations may be used to fit the experimental variation of the plateau currents recorded just after mixing with the cosubstrate concentration (Figure 6). The kinetic characteristics of reaction E_2/E thus obtained are summarized in Table 1. They are in agreement with the spectrophotometric data. The Michaelis−Menten behavior of reaction E_2/E is thus confirmed or, at least, the fact that the reaction is not a mere bimolecular outersphere single electron transfer but rather involves a multistep process showing saturation at high cosubstrate concentration.

Inhibition upon Increasing the H_2O_2 Concentration. Formation and Reduction of the Oxyperoxidase (E_3) Form of the Enzyme. Two pathways for the inactivation of HRP by excess H_2O_2 have been previously identified. One is an irreversible set of reactions finally yielding a verdohemoprotein (also designated as P670).[27] As discussed earlier, this irreversible inactivation pathway of HRP is insignificant under our experimental conditions. The second pathway involves the formation of oxyperoxidase,[28] usually designated as compound III or E_3. This compound, which does not normally participate in the peroxidase activity of HRP, has a structure similar to that of oxyhemoglobin[28b,c] (Scheme 4). In the presence of H_2O_2, the formation of E_3 from the reaction of H_2O_2 with E_2 occurs with a rate constant k_4 ranging from 16 to 40 M^{-1} s^{-1}, depending on pH and temperature.[28d−f] E_3 is not necessarily a dead end to

(27) (a) Nakajima, R.; Yamazaki, I. *J. Biol. Chem.* **1980**, *255*, 2067. (b) Rodriguez-Lopez, J. N.; Hernandez-Ruiz, J.; Garcia-Canovas, F.; Thorneley, R. N. F.; Acosta, M.; Arnao, M. B. *J. Biol. Chem.* **1997**, *272*, 5469.

Scheme 4

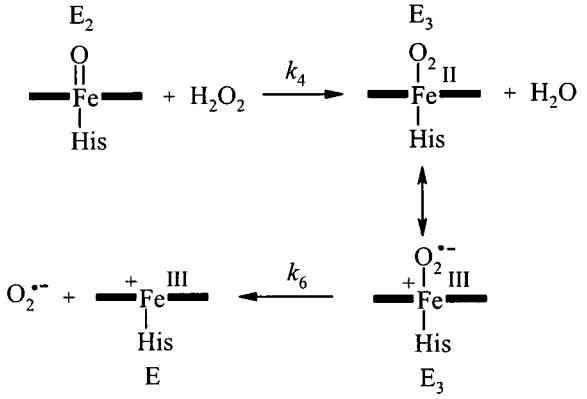

the catalytic cycle of HRP. It is indeed converted back to E by spontaneous decomposition, yielding superoxide ion with a rate constant k_6 ranging from 2.2 to 8.2 × 10^{-3} M^{-1} s^{-1}, depending on pH and temperature.[28a,e,g,k] Also, and more interestingly for the purpose of the present discussion, E_3 has been shown to be reduced to E_1 by several electron donors.[28g−j] It is likely that the osmium(II) complex used as a cosubstrate in the present study may also reduce E_3 to E_1, thus restarting the catalytic cycle of HRP as depicted in Scheme 5.

At the start of the cyclic voltammogram, after an incubation time on the order of 15−20 min, a steady distribution of the enzyme between the inactive form E_3 and the active forms E + E_1 + E_2 is established as defined by

$$[E_3] = C_E^0\left(1 - \frac{k_6}{k_4 C_S^0}\right)$$

$$[E] + [E_1] + [E_2] = C_E^0 \frac{k_6}{k_4 C_S^0} \qquad (9)$$

At low scan rates, an S-shaped wave is observed, which corresponds to a continuously renewed steady distribution of the enzyme over its various forms, having enough time to be established along the potential scan whatever the initial distribution. A second condition for an S-shaped wave to be obtained is that a "pure kinetic" situation be achieved, which is also expected to be the case at low scan rates, as discussed in the Introduction. The occurrence of S-shaped waves additionally requires that the substrate be in concentration large enough not to be significantly consumed in the electrochemical reaction. The voltammograms in Figure 3 indeed illustrate the fact that an uncomplicated S-shaped response tends to prevail at low scan rates. Likewise, the curves displayed in Figure 7, recorded at a very low scan rate (10 mV/s), also show the existence of a plateau above 0.1 mM H_2O_2. The fact that the voltammograms remain reproducible over ca. 1 h confirms the absence of irreversible deactivation during this period of time.

(28) (a) Wittenberg, J. B.; Noble, R. W.; Wittenberg, B. A.; Antonini, E.; Brunori, M.; Wyman, J. *J. Biol. Chem.* **1967**, *242*, 626. (b) Cai, D.; Tien, M. *Biochemistry* **1990**, *29*, 2085. (c) Mylrajan, M.; Valli, K.; Wariishi, H.; Gold, M. H.; Loehr, T. M. *Biochemistry* **1990**, *29*, 9617. (d) Noble, R. W.; Gibson, Q. H. *J. Biol. Chem.* **1970**, *245*, 2409. (e) Nakajima, R.; Yamazaki, I. *J. Biol. Chem.* **1987**, *262*, 2576. (f) Adediran, S. A.; Lambeir, A.-M. *Eur. J. Biochem.* **1989**, *186*, 571. (g) Tamura, M.; Yamazaki, I. *J. Biochem.* **1972**, *71*, 311. (h) Ricard, J.; Job, D. *Eur. J. Biochem.* **1974**, *44*, 359. (i) Odajima, T. *Biochim. Biophys. Acta* **1971**, *235*, 52. (j) Yokota, K.; Yamazaki, I. *Biochem. Biophys. Res. Commun.* **1965**, *18*, 48. (k) Rodriguez-Lopez, J. N.; Smith, A. T.; Thorneley, R. N. F. *J. Biol. Chem.* **1997,** *272*, 389.

Scheme 5

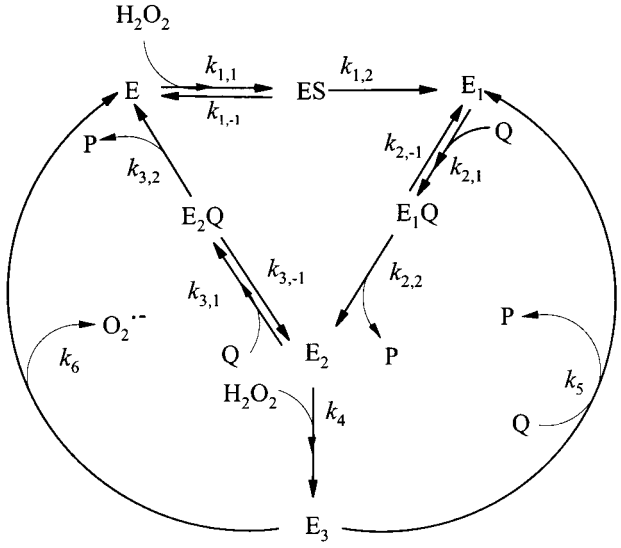

We start testing the validity of the mechanism in Scheme 5 with the results obtained at high H_2O_2 concentrations, 5 and 25 mM, with various concentrations of the cosubstrate under conditions where a plateau current is observed and after an initial steady distribution of the enzyme forms has been established (Figure 8). According to the reaction scheme in Scheme 5, the diffusion reaction kinetics is expressed by eq 10 with the same initial and boundary conditions as those following eq 5.

$$\frac{\partial[Q]}{\partial t} = D_P\frac{\partial^2[Q]}{\partial x^2} - (k_{2,1}[Q][E_1] - k_{2,-1}[E_1Q]) - (k_{3,1}[Q][E_2] - k_{3,-1}[E_2Q]) - k_5[Q][E_3] \qquad (10)$$

Two additional simplifications are introduced at this stage, in agreement with the earlier discussion: (i) reactions E/E_1 and E_1/E_2 are fast as compared to reaction E_2/E, which is thus the rate-determining step of the primary catalytic loop; (ii) a steady-state distribution of the various forms of the enzyme prevails over the whole voltammogram, even though it varies with the electrode potential. Under these conditions, eq 10 simplifies into eq 11 (see Supporting Information). Because the primary

$$\frac{\partial[Q]}{\partial t} = D_P\frac{\partial^2[Q]}{\partial x^2} - \left\{2k_3[Q] + k_4[S]\left(1 + \frac{k_5[Q]}{k_5[Q] + k_6}\right)\right\}[E_2] \qquad (11)$$

catalytic loop is much faster than reactivation, the second kinetic term is negligible as compared to the first for all practical purposes, thus leading to eq 12. In more physical terms, this

$$\frac{\partial[Q]}{\partial t} = D_P\frac{\partial^2[Q]}{\partial x^2} - 2k_3[Q][E_2] \qquad (12)$$

means that the role of reaction E_3/E_1 (k_5) is much more a restarting of the primary catalytic loop deactivated by the conversion of E_2 to E_3 than a direct contribution to the catalytic current. The role of k_5, and of k_4, thus operates through the steady-state value of [E_2], finally leading to the following expression for the plateau current (see Supporting Information):

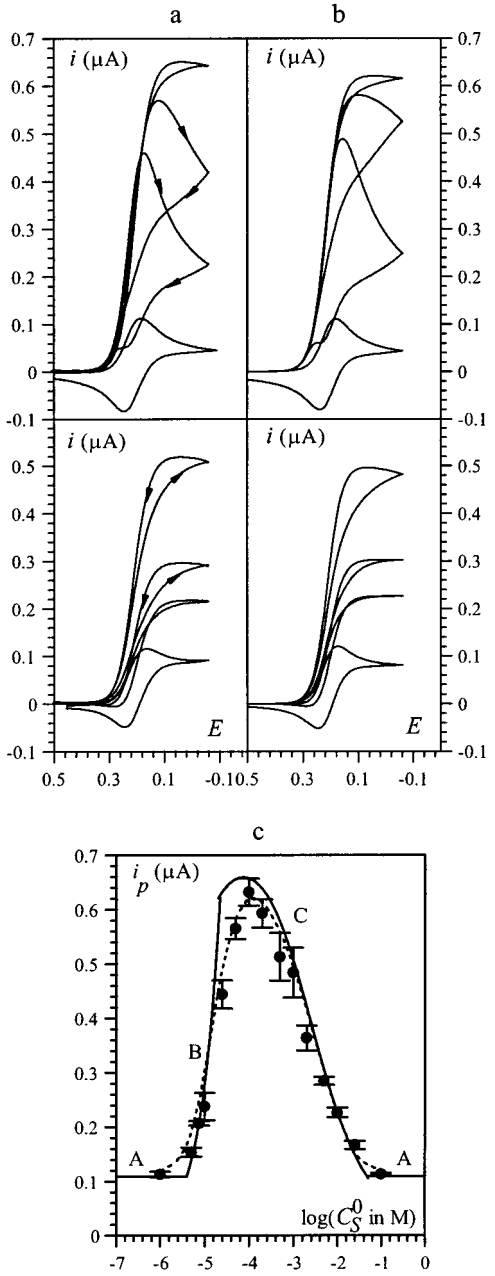

Figure 7. (a) Cyclic voltammograms (scan rate: 10 mV/s) recorded in a phosphate buffer solution (pH 7.4) containing 20 μM $[Os(bpy)_2pyCl]^{2+}$, 0.2 μM HRP, and increasing concentrations of H_2O_2 (upper curves, from bottom to top, 0, 0.025, 0.05, 0.1 mM; lower curves, from top to bottom, 1, 5, 10, 100 mM). (b) Corresponding simulated curves (for details see text). *E* in volts vs SCE. (c) Variation of the peak or plateau (when there is no peak) current with the concentration of H_2O_2. Filled circle symbol: experimental average value of 3−10 measurements per data. Error bar: standard deviation. Full lines: (A) absence of catalysis; (B) control by H_2O_2 diffusion (total catalysis), (C) plateau current according to eq 6. Dotted line: finite difference simulation.

$$i_{\mathrm{pl}} = FSC_{\mathrm{P}}^0\sqrt{D_{\mathrm{P}}}\sqrt{2k_3C_{\mathrm{E}}^0}\,\mathrm{lms}(\chi,\rho,\epsilon) \qquad (13)$$

with

$$\chi = \frac{K_{3,\mathrm{M}}}{C_{\mathrm{P}}^0}, \quad \rho = \frac{k_4C_{\mathrm{S}}^0}{k_5C_{\mathrm{P}}^0}, \quad \text{and} \quad \epsilon = \frac{k_6}{k_5C_{\mathrm{P}}^0}$$

where $\mathrm{lms}(\chi,\rho,\epsilon)$ is the function defined in the Supporting Information, $F = 96\,487$ C, $S = 0.0962$ cm^2, and $D_{\mathrm{P}} = (4.5 \pm 0.4) \times 10^{-6}$ cm^2 s^{-1} (voltammetric determination).

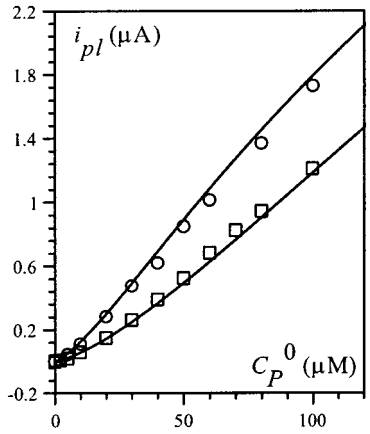

Figure 8. Catalytic plateau current as a function of the cosubstrate concentration recorded at 10 mV s^{-1} after an incubation time of 20 min in a phosphate buffer (pH 7.4) containing 0.2 μM HRP, 5 (○) and 25 (□) mM H_2O_2. Full line: fitting with eq 13 with $k_3 = 1.4 \times 10^7$ M^{-1} s^{-1}, $K_{3,\mathrm{M}} = 20$ μM, $k_4/k_5 = 0.029$, $k_6/k_5 = 6.3$ μM.

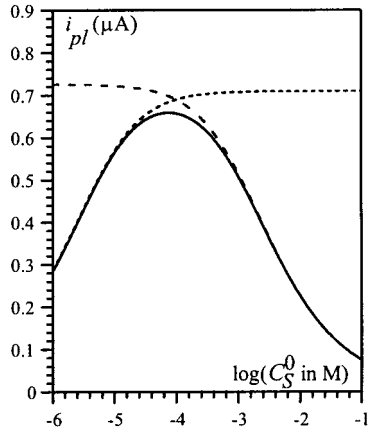

Figure 9. Variation of the plateau current with the concentration of H_2O_2 under the same conditions as in Figure 7. Dashed line: effect of inhibition according to eq 13. Dotted line: effect of the kinetic control of the primary catalytic loop by reaction E/E_1 according to eq 6. Full line: both effects present according to eqs 13 and 15.

Equation 13 was used to fit the data obtained at large H_2O_2 concentrations that are represented in Figure 8. The proportionality coefficient between i_{pl} and (χ,ρ,ϵ) was obtained from the previously derived value of k_3, while χ was obtained at each value of C_{P}^0 from the value of $K_{3,\mathrm{M}}$. The data in Figure 8 thus provide a relationship between ρ and ϵ. This is the start of the iteration procedure finally leading to k_4, k_5, and k_6. The fitting curve in Figure 8 was drawn for the values of the three constants obtained once the iteration process has been completed. It shows that there is an excellent agreement between theory and experiment.

The variation of the plateau current with the concentration of H_2O_2 under the same conditions may also be obtained from eq 13. It is represented by the dashed line in Figure 9, showing how the increase in H_2O_2 concentration results in more and more inhibition and, consequently, in smaller and smaller plateau currents.

Going to the lower end of the range of H_2O_2 concentrations, eq 13 becomes less and less applicable because the approximation that reaction E_2/E is the sole rate-determining step in the

primary catalytic cycle becomes less and less valid. Since inhibition tends to vanish as the H_2O_2 concentration decreases, the i_{pl} vs H_2O_2 concentration plot tends asymptotically toward the curve defined by eq 6, represented by the dotted line in Figure 9. Along this curve, i_{pl} tends to vary in proportion to the square root of H_2O_2 concentration (eq 14) as it becomes smaller and smaller, in line with the fact that reaction E/E_1 tends to then become the rate-determining step of the primary catalytic loop.

$$i_{pl} = FS\sqrt{D_P}\sqrt{4k_1C_E^0C_P^0}\sqrt{C_S^0} \qquad (14)$$

It is also worth noting that the dotted line tends toward a horizontal asymptote upon increasing the H_2O_2 concentration. This means that if inhibition had been absent, the electrochemical response would have then become independent of the concentration of H_2O_2.

Between the two limiting behaviors, the i_{pl} vs C_S^0 variation is depicted by the solid line in Figure 9, which is constructed from eq 13, replacing χ by χ' (eq 15) while ρ and ϵ remain unchanged (see Supporting Information).

$$\frac{1}{\chi'} = \frac{1}{\chi} + k_3C_P^0\left(\frac{1}{k_{1,2}} + \frac{1}{k_1C_S^0}\right) \qquad (15)$$

Substrate Diffusion Control at Very Low H_2O_2 Concentrations. At very low H_2O_2 concentrations, why do the cyclic voltammograms exhibit a scan-rate-dependent irreversible peak rather than a scan-rate-independent plateau (Figures 2a, 7a)? Why is the peak current then proportional to the concentration of H_2O_2 rather than to its square root (Figures 2c, 7c)? These are the two questions we address now.

One of the conditions required for a plateau current to be observed is that the concentration of substrate is large enough for its consumption in the reaction−diffusion layer to be regarded as negligible.[21] As long as this condition is met, the diffusion of H_2O_2 from the solution to the electrode does not interfere in the current flowing through the electrode surface. As the concentration of H_2O_2 is made smaller and smaller, this condition is less and less fulfilled, and therefore, the diffusion of H_2O_2 comes into play. Thus, as long as the concentration of H_2O_2 is not small enough to make the catalytic effect vanish, the conditions for "total catalysis" are obeyed, giving rise to an irreversible peak whose height is given (see Supporting Information) by eq 16.[20b,c]

$$i_p = 2\left(0.609FS\sqrt{D_S}C_S^0\sqrt{\frac{F\nu}{RT}}\right) \qquad (16)$$

In summary, the variation of the peak current or plateau current (when there is no peak) with the concentration of H_2O_2 in the absence of inhibition is plotted in Figure 10, which shows the successive limiting behaviors and the passage from one to the other. The intermediate segments were computed by a finite difference numerical technique (Digisim).

Hysteresis and Trace Crossing. Figures 2 and 7 show several examples of hysteresis and trace crossing. As compared to the canonical "purely catalytic" S-shaped wave, the reaching

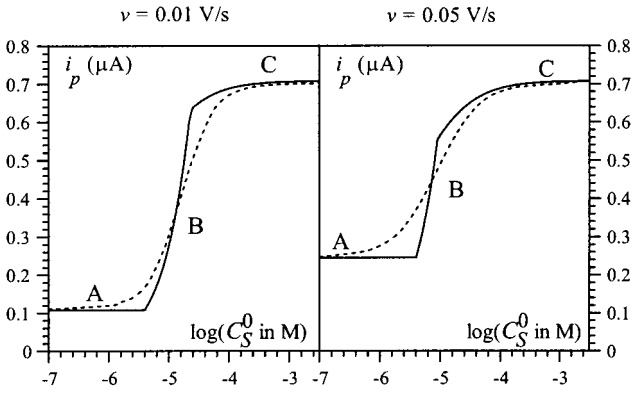

Figure 10. Variation of the peak or plateau (when there is no peak) current with the concentration of H_2O_2 in the absence of inhibition. Same conditions as in Figures 7 and 2, respectively. Full lines: limiting behaviors for (A) absence of catalysis; (B) control by H_2O_2 diffusion (total catalysis); (C) plateau current according to eq 6. Dashed line: passage from one limiting situations to the other.

of the plateau current seems to drag on along the potential (and time) axis during the forward scan. The increase of the current with time continues in the first part of the reverse scan, followed by a crossing of the anodic trace with the cathodic trace.

These phenomena, which become more and more apparent upon raising the scan rate until the catalytic phenomenon vanishes, arise from the combined action of two factors. Hysteresis is related to the time required by the intervening forms of the enzyme to reach a steady-state potential-dependent distribution. In other words, the steady-state assumption that we have made so far should be removed. Trace crossing, which is almost absent at the lowest scan rate, becomes more and more apparent as the scan rate increases. It is caused by the fact that "pure kinetic" conditions are less and less satisfied, meaning that the diffusion of Q controls more and more the dynamics of the system. It is difficult to observe the two phenomena separately because a decrease of the scan rate, aimed at a better achievement of the pure kinetic conditions, has simultaneously the consequence that more time is available for the steady-state distribution of the enzymes to be reached. The best approximation of a pure hysteresis effect is provided by the curves obtained at 0.01 V s^{-1} in the conditions of Figures 3, 7, and 11.

The hysteresis effect will be described in more detail further on. For the moment we may simulate the combination of the two effects by means of a finite difference resolution of the partial derivative equation pertaining to Q with the attending initial and boundary conditions (we used the Digisim package for this purpose). Among the latter conditions, the enzyme distribution at the start of the potential scan is given by eqs 9. k_6 interferes in the dynamics of the system in two ways. A relatively minor contribution, which we have already invoked, relates to the competition of k_6 with k_5[Q] in the regeneration of E from E_3. The other, more important factor is the control of the initial distribution of enzyme according to eq 9. Thus, if we wish, in a second step of the iteration procedure, to minimize the interference of k_6, we may first simulate the data obtained at high concentrations of H_2O_2, high enough for the entire enzyme to be under the E_3 form at time zero. This is the case for the experiments summarized in Figure 11, which will be confirmed after the iterative determination of the rate constants has been completed. The simulated voltammograms in Figure 11b correspond to the values of k_4, k_5, and k_6 that have been

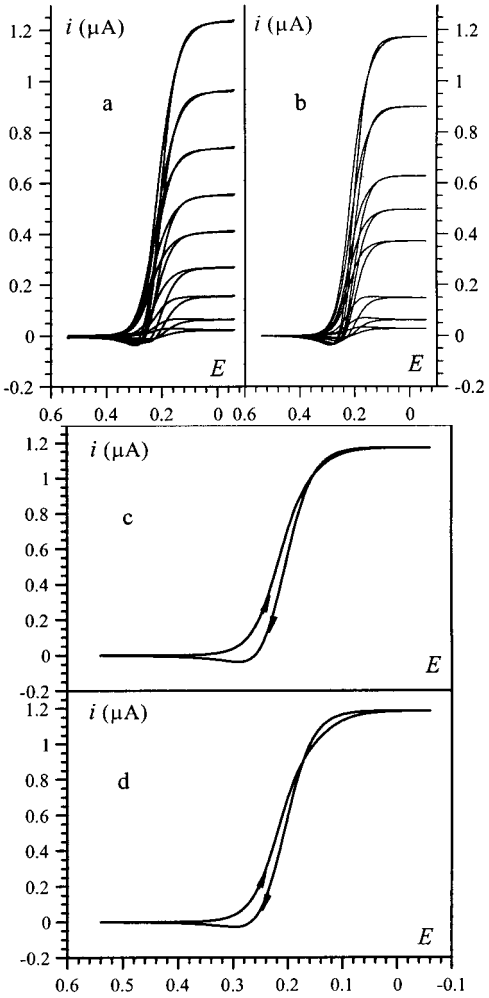

Figure 11. (a) Cyclic voltammograms (scan rate: 10 mV/s) recorded (after attainment of steady state before starting the potential scan) in a phosphate buffer solution (pH 7.4) containing 25 mM H_2O_2, 0.2 μM HRP, and increasing concentrations of $[Os(bpy)_2pyCl]^{2+}$. From bottom to top: 5, 10, 20, 30, 40, 50, 60, 80, 100 μM. (b) Simulated curves obtained with $k_1 = 1.7 \times 10^7$ M^{-1} s^{-1}, $K_{1,M} = 128$ μM, $k_2 \gg k_1$, $k_3 = 1.4 \times 10^7$ M^{-1} s^{-1}, $K_{3,M} = 20$ μM, $k_4 = 55$ M^{-1} s^{-1}, $k_5 = 1900$ M^{-1} s^{-1}, $k_6 = 0.012$ s^{-1}. (c) Simulated curve for 100 μM cosubstrate with the same values of the kinetic characteristics as in (b). (d) As in (c), except that the values of k_4, k_5, and k_6 have been lowered by 30%, keeping constant the ratios k_4/k_5 and k_6/k_5.

obtained at the end of the iterative procedure, showing an excellent agreement between the experimental and theoretical curves. Figure 11c,d illustrates that a small change of k_4, keeping constant the ratios k_4/k_5 and k_6/k_5, alters appreciably the reproduction of the hysteresis and trace crossing phenomena, although they are not large in these experiments, leading to the conclusion that the values of the rate constants could be determined with a good accuracy.

We may now end the iterative determination of the rate constants with the simulation of experiments carried out with a concentration of H_2O_2 where a larger fraction of the enzyme is in the E_2 form under the steady-state conditions prevailing at the start of the scan, as it is the case in the experiments summarized in Figures 3 and 7. The best fitting obtained for all three steps of the iteration procedure thus led to $k_4 = 55$ M^{-1} s^{-1}, $k_5 = 1900$ M^{-1} s^{-1}, and $k_6 = 0.012$ s^{-1}, with an accuracy of ca. 30% for each rate constant. Under the conditions given in Figure 11, eqs 9 show that 99% of the enzyme is in the E_3 form, thus confirming the above assumption that it is practically the sole form of the enzyme present in the initial contribution. The value of k_5 was corroborated by an independent approach. It consists of generating E_3 by the dihydroxyfumarate method [28j] and following spectrophotochemically the oxidation of $[Os(bpy)_2pyCl]^+$ by E_3. A value of 1700 ± 500 M^{-1} s^{-1} was thus obtained.

Although the good fit between the simulated and experimental curves provides satisfactory evidence of the validity of the mechanism depicted in Scheme 5, it is worth examining in more details what causes the hysteresis and trace crossing phenomena.

Modeling of the first of them, with no interference of the second, involves considering the variation of the concentration of the various forms of the enzyme with time, given that the "pure kinetic" conditions are assumed to be operative. In the domain of H_2O_2 concentrations where hysteresis appears, reaction E_2/E is the sole rate-determining step of the primary catalytic loop. E_2, E_2Q, and E_3 are thus the only forms we need consider, thus leading to eqs 17, with eqs 9 as initial conditions.

$$\frac{d[E_2]}{dt} = -k_{3,1}[Q][E_2] + (k_{3,-1} + k_{3,2})[E_2Q] - k_4C_S^0[E_2] + (k_5[Q] + k_6)[E_3]$$

$$\frac{d[E_2Q]}{dt} = k_{3,1}[Q][E_2] - (k_{3,-1} + k_{3,2})[E_2Q] \qquad (17)$$

$$\frac{d[E_3]}{dt} = k_4C_S^0[E_2] - (k_5[Q] + k_6)[E_3]$$

Fulfillment of the "pure kinetic" conditions implies that, in eq 12, $\partial[Q]/\partial t = 0$. It follows that [Q] is independent of time and may be equated to $[Q]_{x=0}$ in eqs 17, while $[E_2]$, $[E_2Q]$, and $[E_3]$ do depend on time but not on the distance to the electrode surface. For each of the three forms of the enzyme, we may thus derive the variation of its concentration with time until the steady state is reached by integration of eqs 17 with eqs 9 as initial conditions. For example, the variation of $[E_2]$ with time is as depicted by eq 18 (see Supporting Information), with the same definitions of χ, ρ, and ϵ as in eq 13.

$$\frac{[E_2]}{C_E^0} = \frac{[E_2]_{t=0}}{C_E^0}\frac{1}{1+\frac{q_{x=0}}{\chi}} \times \exp\left\{-\left(\frac{1}{1+\frac{q_{x=0}}{\chi}} + \frac{q_{x=0}+\epsilon}{\rho}\right)k_4C_S^0t\right\} + \frac{1}{1+\frac{q_{x=0}}{\chi}+\frac{\rho}{q+\epsilon}} \times \left[1 - \exp\left\{-\left(\frac{1}{1+\frac{q_{x=0}}{\chi}} + \frac{q_{x=0}+\epsilon}{\rho}\right)k_4C_S^0t\right\}\right] \qquad (18)$$

$$(q_{x=0} = [Q]_{x=0}/C_P^0)$$

An example of the delayed establishment of steady state between these three forms of the enzyme is shown in Figure 12, where the variation of $[E_2]$ along the cyclic voltammogram

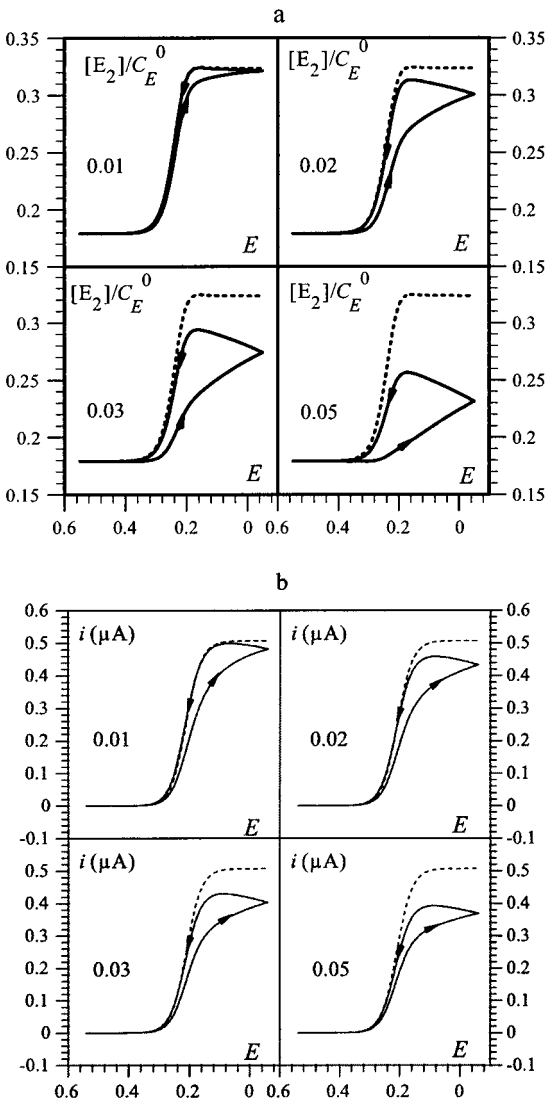

Figure 12. Delayed establishment of steady state between the various forms of the enzyme under the same experimental conditions as in Figure 3. The number indicated in each diagram is the scan rate in volts per second. (a) Variation of the concentration of E_2 with potential. Dashed line: steady-state conditions. (b) Predicted cyclic voltammograms in the absence of kinetic control of cosubstrate diffusion, i.e., under the conditions prevailing in (a).

(12a) and the cyclic voltammograms themselves (12b) are represented for several values of the scan rate. As seen on the latter curves, this factor accounts for the observed hysteresis but not for trace crossing. The latter effect thus requires the interference of Q diffusion in the dynamics of the whole process.

Mechanism Overview. Tests of Self-Consistency. The various pieces of information that we have gathered may now be put together to provide a comprehensive picture of the mechanism of mediated electrochemistry of HRP. We may conclude that it follows the reaction scheme in Scheme 5 associated with the values of the various kinetic constants summarized in Table 2. For the constants that have previously been measured, we see that there is a good agreement with the values determined in this work.

We may also use these various rate constants to simulate the "calibration curves" relating the electrochemical responses to the concentration of H_2O_2, such as those represented in Figures 2c and 7c for a scan rate of 50 and 10 mV s^{-1}, respectively.

Table 2. Kinetic Characteristics of the Mediated Electrochemistry of HRP (Scheme 5)

reaction	kinetic characteristics [a]
$E + H_2O_2/E_1$ [b]	$k_1 = 1.7 \times 10^7$, $k_{1,2} = 2.2 \times 10^3$, $K_{1,M} = 128$
$E_1 + Q/E_2$	$k_2 = 2 \times 10^8$
$E_2 + Q/E$	$k_3 = 1.4 \times 10^7$, $k_{3,2} = 2.8 \times 10^2$, $K_{3,M} = 20$
$E_2 + H_2O_2/E_3$ [c]	$k_4 = 55$
$E_3 + Q/E_1$	$k_5 = 1.9 \times 10^3$
E_3/E [c]	$k_6 = 1.2 \times 10^{-2}$

[a] At pH 7.4 and 20 °C, first-order rate constants in s^{-1}, bimolecular rate constants in M^{-1} s^{-1}, K_M's in μM. [b] From ref 2f. [c] Literature values: $k_4 = 40$,[28d] $k_6 = 0.8 \times 10^{-2}$.[28j]

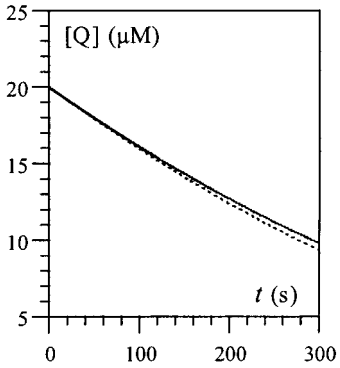

Figure 13. Simulated decay of the osmium(II) concentration with time during the steady-state spectrophotometic experiment involving 0.2 nM HRP, 20 μM osmium(II), and 0.1 mM H_2O_2. Plain line: in the presence of the E_2/E_3 reaction. Dashed line: in the absence of the E_2/E_3 reaction.

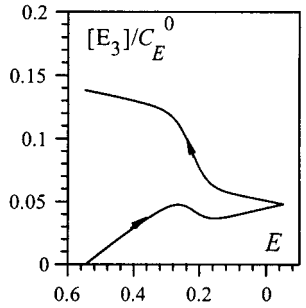

Figure 14. Predicted formation of E_3 along the cyclic voltammogram under the same conditions as in Figure 6.

We note in this connection that the final simulation is closer to the curves representing the various successive regimes at 10 mV s^{-1} than at 50 mV s^{-1}. This is because the system is closer to the "pure kinetic" situation at the lowest scan rate.

Since we now know the whole set of kinetic characteristics, we may proceed with the tests of self-consistency of the experiments in which the E_2/E reaction was kinetically characterized under the assumption that conversion of E_2 into the inactive form E_3 could be regarded as negligible. These tests concern first the *steady-state spectrophotometric experiments*. Simulation of the decay of the cosubsrate concentration within the time window of the experiment with and without the interference of the E_2/E_3 reaction (Figure 13) shows that the formation of E_3 is indeed negligible within the concentration range of H_2O_2 we selected to investigate the primary catalytic cycle.

The same conclusion applies to the *cyclic voltammetric experiments*, as depicted in Figure 14, which represents the formation of E_3 under the conditions that we selected to

investigate the primary catalytic cycle with negligible inhibition, according to eq 19 (see Supporting Information).

$$e_3 = e_3^0 \exp\{-(k_5 C_P^0 q_{x=0} + k_6)t\} + e_2^0 \left[\exp\{-(k_5 C_P^0 q_{x=0} + k_6)t\} - \exp\left\{ -\left(\frac{k_4 C_S^0}{1 + \frac{q_{x=0}}{\chi}} + k_5 C_P^0 q_{x=0} + k_6 \right) t \right\} \right] + \frac{\frac{k_4 C_S^0}{1+\chi} - \left(\frac{k_4 C_S^0}{1 + \frac{q_{x=0}}{\chi}} + k_5 C_P^0 q_{x=0} + k_6 \right) \exp\{-(k_5 C_P^0 q_{x=0} + k_6)t\}}{\left(\frac{k_4 C_S^0}{1 + \frac{q_{x=0}}{\chi}} + k_5 C_P^0 q_{x=0} + k_6 \right)} + \frac{(k_5 C_P^0 q_{x=0} + k_6) \exp\left\{ -\left(\frac{k_4 C_S^0}{1 + \frac{q_{x=0}}{\chi}} + k_5 C_P^0 q_{x}{=}0 + k_6 \right) t \right\}}{\left(\frac{k_4 C_S^0}{1 + \frac{q_{x=0}}{\chi}} + k_5 C_P^0 q_{x=0} + k_6 \right)} \quad (19)$$

Starting from a negligible amount of E_3 at the foot of the voltammetric wave, Figure 14 shows that the formation of E_3 during the cathodic scan remains below 5% of the total amount of enzyme and can therefore be regarded as negligible in the determination of the rate characteristics based on the height of the current plateau as depicted earlier.

Conclusions

The systematic analysis of the cyclic voltammetric responses as a function of the scan rate and of the substrate and cosubstrate concentrations, complemented by steady-state and stopped-flow experiments, allowed a precise determination of the complex mechanism of catalysis and inhibition involved in the reaction of HRP with H_2O_2 as substrate and an outersphere single electron donor as cosubstrate.

The variation of the electrochemical response with the substrate concentration is, at first sight, perplexing. While for very small concentrations of H_2O_2, the response increases, as expected, with H_2O_2 concentration, a maximum and a descending variation are rapidly observed. This behavior is caused by the reaction of the E_2 form of the enzyme with H_2O_2, forming oxyperoxidase (E_3), which inhibits catalysis. In the framework of the mechanism represented in Scheme 5, conditions can be defined (low H_2O_2 concentrations, rapid recording of the voltammogram) which render inhibition insignificant. An electrochemical analysis of the primary catalytic cycle, which rotates between the E, E_1, and E_2 forms of the enzyme, is thus allowed, leading to the determination of the rate constant of the reaction between E_2 and the reduced form of the cosubstrate. The reductions of E_1 and E_2 by $[Os(bpy)_2pyCl]^+$ are remarkably fast compared to other electron donors, up to 10-fold faster than many natural phenolic cosubstrates,[2f,25] making this osmium(II) complex one of the most reactive cosubstrates to HRP. It is worthy of notice that Michaelis−Menten-type kinetics is found for the latter reaction, showing a tendency toward saturation as the cosubstrate concentration increases. This observation and the fact that an electrochemical method is henceforth available for a kinetic characterization of the reaction should prove important in further studies aiming at a more detailed depiction of its mechanism and reactivity patterns to be pursued by systematic investigation of properly designed families of cosubstrates.

At very low concentrations of H_2O_2, its consumption within the reaction−diffusion layer may no longer be neglected, leading to a situation where its diffusion toward the electrode surface partly controls the catalytic current. The cyclic voltammetric response then exhibits an irreversible peak rather than the classical plateau-shaped wave observed at higher concentrations. When complete diffusion control is reached, the electrochemical response is proportional to H_2O_2 concentration, in contrast to the square root dependence associated with plateau-shaped responses.

Inhibition interferes more and more with increasing H_2O_2 concentration. It is caused by the formation of oxyperoxidase (E_3) from the reaction of E_2 with H_2O_2. However, E_3 is not a dead end to the catalytic process, since not only does it decompose slowly into the native peroxidase (E) and superoxide ion, but it also reacts on the reduced form of the cosubstrate to regenerate the E_1, thus starting again the primary catalytic cycle. Analysis of the electrochemical responses thus allows the determination of the rate constant of this reaction. An avenue is thus opened to a detailed analysis of its mechanism and reactivity patterns by means of properly designed families of cosubstrates in this case, too.

The fact that a bell-shaped calibration curve relates the electrochemical response to the concentration of H_2O_2 should be taken into account in biosensor applications. The analysis and data provided here allow one to predict the amperometric response in all practical cases.

Intriguing hysteresis and trace crossing behaviors have also been quantitatively explained. Hysteresis results from the delay time required for the various forms of the enzyme to reach a steady state. Trace crossing results from the additional interference of cosubstrate diffusion in the control of the current.

Experimental Section

Reagents. Lyophilized HRP (mainly composed of isoenzyme C) was purchased from Sigma (type VI; RZ = 3.1) and used without further purification. The concentration of HRP was determined spectrophotometrically using the Soret extinction coefficient of 102 mM^{-1} cm^{-1} at 403 nm. $[Os(bpy)_2pyCl]PF_6$ was synthesized as previously described,[29] and its oxidized form was obtained by chemical oxidation with $AgPF_6$ obtained from Aldrich. Hydrogen peroxide (50%) was supplied by Prolabo as reagent grade, and its concentration was determined by permanganate titration. The phosphate buffer (PB, 4.3 mM NaH_2PO_4, 15.1 mM Na_2HPO_4, and 50 mM NaCl, pH 7.4) and all of the other aqueous solutions were prepared using water purified by a Milli-Q water purification system from Millipore.

Steady-State Kinetics of the Reaction of HRP with Os^{III}. A Hewlett-Packard 8452 diode array spectrophotometer interfaced with a personal computer was used for UV−visible absorbance measurements. Steady-state kinetics were studied by measuring the initial rates of $[Os(bpy)_2pyCl]^+$ oxidation at 20 °C as a function of reducing substrate concentration. Osmium(II) consumption was followed at 500

(29) Kober, E. M.; Caspar, J. V.; Sullivan, B. P.; Meyer, T. J. *Inorg. Chem.* **1988**, *27*, 4587.

nm ($\epsilon_{500\ nm} = 8.7\ mM^{-1}\ cm^{-1}$). The reactions were initiated by addition of H_2O_2 (final concentration of 0.1 mM) to a mixture of HRP (0.2 nM) and $[Os(bpy)_2pyCl]^+$ (ranging from 0.2 μM to 0.15 mM) in PB.

Spectrophotometric Measurements of k_5. The method is similar to the one given in ref 28j. Oxyperoxidase was generated in situ in the cell of the spectrophotometer by the addition of 6 equiv of dihydroxyfumarate and 0.5 equiv of H_2O_2 to the aerobic solution of 1 equiv of HRP (final concentration of 4 μM in a 0.1 M citrate buffer, pH 5.0, 20 °C). Once the dihydroxyfumarate was completely consumed, a concentration ranging from 0.5 to 2 equiv of osmium(II) in a 0.1 M citrate buffer was added, and the kinetic decay of E_3 was monitored at 418 nm.

Pre-Steady-State Kinetics Measurements. Stopped-flow measurements were performed with a three-syringe SFM300 sequential-mix instrument (Biologic, Grenoble, France) equipped with a 75-W Xe lamp source and a fast diode array spectrophotometer (J&M Tidas, Germany). The drive syringes and the reaction cell were maintained at 20 °C using a circulating water bath. The reduction of E_1 by osmium(II) was monitored at 411 nm (isobestic point between the Soret bands of E and E_2). E_1 was formed by mixing 1 equiv of HRP and H_2O_2 in the aging delay line (1 s delay time) with the use of the first two syringes, and it was next reduced by the addition of 1 equiv of osmium(II) using the third syringe (the final concentration of each of the three components in the cell was 0.5 μM). The reduction of E_2 by osmium(II) was monitored at 427 nm (isobestic point between the Soret bands of E and E_1). E_2 was prepared by mixing 1 equiv of E with a mixture of 1 equiv of H_2O_2 and 0.9 equiv of ascorbic acid in the aging delay line (1 s delay time), and it was next reduced by the addition of 1 equiv of osmium(II) using the third syringe (final concentration of 1 μM). Both processes followed second-order kinetics, and the observed rates were determined by nonlinear least-squares fitting. The resulting second-order rate constant values were obtained from the average of four separate experiments.

Electrochemical Experiments. An EG&G PAR potensiostat interfaced to a personal computer was used for cyclic voltammetry (CV). Carbon-based screen-printed electrodes (9.6 mm^2 for the sensing disk area) were used as disposable working electrodes, and they were prepared as described previously[30] from a homemade carbon-based ink composed of graphite particles (Ultra Carbon, UCP 1M, Johnson Matthey) and polystyrene, using a manual screen-printer (Circuit Imprimé Français, Bagneux, France) equipped with a screen stencil of 77 threads cm^{-1}. A saturated calomel electrode (SCE) or an Ag/AgCl electrode was employed as reference. The potentials indicated in the text are referred to the SCE. The counter electrode was a platinum wire. The experiments were performed in a water-jacketed electrochemical cell maintained at 20 ± 0.5 °C with a circulating water bath. To avoid the catalytic contribution of HRP absorbed onto the electrode surface during prolonged immersion time, a new screen-printed electrode was used for each experiment.

Simulations of the cyclic voltammograms were carried out with DigiSim software from Bioanalytical Systems Inc. (West Lafayette, IN). The enzyme was then considered as practically immobile as compared to the cosubstrate (diffusion coefficients: $10^{-10}\ cm^2\ s^{-1}$ for the enzyme vs $5 \times 10^{-6}\ cm^2\ s^{-1}$ for the cosubstrate). The diffusion coefficient of H_2O_2 was taken equal to $1.6 \times 10^{-5}\ cm^2\ s^{-1}$.[31]

Supporting Information Available: Derivation of eqs 3, 6, 11, 13, 15, 16, 18, and 19 (PDF). This material is available free of charge via the Internet at http://pubs.acs.org.

JA0170706

(30) Bagel, O.; Limoges, B.; Schöllhorn, B.; Degrand, C. *Anal. Chem.* **1997**, *69*, 4688.
(31) Prabhu, V. G.; Zarapkar, L. R.; Dhaneshwar, R. G. *Electrochim. Acta* **1981**, *26*, 725.